Exotic break-up modes in heavy ion reactions at low energies

C. Rizzo,[1] M. Colonna,[1] V. Baran,[2] and M. Di Toro[1,3]
[1]*INFN-LNS, Laboratori Nazionali del Sud, 95123 Catania, Italy*
[2]*Faculty of Physics, University of Bucharest, 077125 Bucharest, Romania*
[3]*Physics and Astronomy Department, University of Catania, 95123 Catania, Italy*
(Received 3 July 2014; revised manuscript received 21 October 2014; published 21 November 2014)

New reaction mechanisms occurring in heavy ion collisions at low energy (10–30 MeV/nucleon) are investigated within the stochastic mean field model. We concentrate on the analysis of ternary breakup events, of dynamical origin, occurring in semicentral reactions, where the formation of excited systems in various conditions of shape and angular momentum is observed. We show how this fragmentation mode may emerge from the combined action of surface (neck) instabilities and angular momentum effects. Interesting perspectives on this mechanism in neutron-rich (or exotic) systems are developing, with the possibility of accessing information on the low-density behavior of the nuclear symmetry energy.

DOI: 10.1103/PhysRevC.90.054618 PACS number(s): 25.70.Lm, 21.30.Fe, 24.60.Ky, 25.70.Mn

I. INTRODUCTION

At energies from just above the Coulomb barrier up to the Fermi regime, heavy ion collisions are largely dominated by dissipative one-body reaction mechanisms. According to the selected impact parameter window, the reaction dynamics ranges mainly from (incomplete) fusion to binary channels, associated with deep inelastic and/or dynamical fission processes [1]. Owing to the complex mean-field dynamics, the system may explore, along the separation path, rather extreme conditions with respect to shape and angular momentum, which may induce large fluctuations in the exit channel. The mechanisms governing the transition between fusionlike and binarylike processes represent a long-lasting subject of investigation [2–4]. In particular, much attention has been devoted to the possible origin of the large variances observed for the reaction products [2,3,5–7].

The very dissipative dynamics may also lead, especially in collisions between medium-heavy systems, to the development of new modes of reseparation, such as dynamical ternary or quaternary breaking. The occurrence of this reaction outcome, characterized by massive fragments nearly aligned along a common separation axis, is well documented [8,9] and has been recently reported in ^{197}Au + ^{197}Au collisions at 15 and 23 MeV/nucleon [10–12]. The intricate neck dynamics and the formation of rather elongated projectile-like (PLF) and target-like (TLF) fragments, in semiperipheral reactions, could be at the origin of further rupture steps, leading to the observation of three or four fragments in the exit channel. Large-scale quantum and thermal fluctuations of the nuclear mean field are expected to play a crucial role in this process, thus opening the possibility to learn about important ingredients of the nuclear effective interaction [7].

Another interesting aspect is connected to the transition from the ternary breakup channel to the neck fragmentation mechanism observed at higher beam energies. Indeed, in semiperipheral collisions at 30–50 MeV/nucleon, the low-density neck region which develops between the two reaction partners becomes so pronounced that small fragments are directly emitted on very short time scales, with larger relative velocity with respect to PLF and TLF [13–17].

In reactions involving neutron-rich (or even exotic) nuclei, one may expect the multibreakup probability to be affected by the dynamics of the neutron-rich neck region, which, in turn, can be influenced by specific properties of the nuclear effective interaction. Indeed from these studies it may become possible to access information on the low-density behavior of the isovector term of the nuclear potential [18] and the corresponding symmetry energy of the nuclear equation of state, on which many investigations are concentrated nowadays; see Ref. [19] for a recent review.

From the above discussion, it is clear that a detailed analysis of the mean-field dynamics, and associated shape fluctuations and rotational effects, is crucial to investigate the competition between reaction mechanisms as well as the nature of new exotic reseparation modes, in low-energy dissipative collisions. In this paper, we undertake such a study in the framework of the stochastic mean field (SMF) transport model, which has been shown to provide a good description of mean-field dynamics and incorporates effects of two-body fluctuations and correlations [20–23]. We will investigate semiperipheral heavy ion collisions in the beam energy range of 10–30 MeV/nucleon, focusing on the possible occurrence of ternary breaking and the features of the associated reaction products. This analysis may open a novel understanding of the transition path from deep inelastic collisions to multifragmentation processes and elucidate the nuclear dissipation mechanisms.

The paper is organized as it follows: In Sec. II we present the SMF transport treatment employed to follow the dynamical evolution of nuclear collisions. Results concerning the features of multistep breaking mechanisms are discussed in Sec. III. Finally conclusions and perspectives are drawn in Sec. IV.

II. DYNAMICAL DESCRIPTION OF NUCLEAR REACTIONS

The description of the nuclear reaction dynamics is afforded considering, as a starting point, the Boltzmann-Langevin (BL) equation, which defines the time evolution of the semiclassical one-body distribution function $f(\mathbf{r},\mathbf{p},t)$ (i.e., the semiclassical analog of the Wigner transform of the one-body density

matrix):

$$\frac{\partial f}{\partial t} + \frac{\mathbf{p}}{m}\frac{\partial f}{\partial \mathbf{r}} - \frac{\partial U}{\partial \mathbf{r}}\frac{\partial f}{\partial \mathbf{p}} = I_{\rm coll}[f] + \delta I[f]. \quad (1)$$

The coordinates of isospin are not shown for brevity. Equation (1) essentially describes the behavior of the system in response to the action of the self-consistent mean-field potential U, whereas effects of two-body correlations and fluctuations are incorporated in the collision integral, $I_{\rm coll}$, and its stochastic part, δI [24,25]. The average term $I_{\rm coll}[f]$ takes into account the energy, angular, and isospin dependence of free nucleon-nucleon cross sections [26].

We adopt the following parametrization of the mean-field potential:

$$U_q = A\frac{\rho}{\rho_0} + B\left(\frac{\rho}{\rho_0}\right)^{\alpha+1} + C\frac{\rho_n - \rho_p}{\rho_0}\tau_q, \quad (2)$$

where ρ denotes the density, $q = n, p$, and $\tau_n = 1, \tau_p = -1$. The coefficients $A = -356$ MeV, $B = 303$ MeV, and the exponent $\alpha = \frac{1}{6}$, characterizing the isoscalar part of the mean field, are fixed requiring that the saturation properties of symmetric nuclear matter, $\rho_0 = 0.16\ {\rm fm}^{-3}$ and $E/A = -16$ MeV/nucleon, with a compressibility of 200 MeV, are reproduced. We notice that the considered compressibility value is favored, e.g., from flow, monopole oscillation, and multifragmentation studies [20,27]. This choice corresponds to a Skyrme-like effective interaction, namely SKM^*, for which we consider the effective mass as being equal to the nucleon bare mass. As far as the isovector part of the nuclear interaction is concerned, we take a constant value of $C = 36$ MeV, corresponding to a linear (stiff) behavior of the potential part of the symmetry energy, $C_{\rm sym}^{\rm pot} = 36\rho/(2\rho_0)$ [21,26].

Within such a framework, the system is described in terms of the one-body distribution function f, but this function may experience a stochastic evolution in response to the action of the fluctuating term $\delta I[f]$. The stochastic mean field (SMF) model that we adopt here represents an approximate approach to solve the BL equation, where phase-space fluctuations are projected in coordinate space [28,29]. Thus the fluctuating term $\delta I[f]$ is implemented through stochastic spatial density fluctuations. Equation (1) is solved numerically, adopting the test particle method [28].

It should be noticed that semiclassical models have been shown to work well for the description of the approaching phase of reactions at energies just above the Coulomb barrier, leading to the formation of composite excited systems [30–32]. Moreover, the inclusion of fluctuations in the dynamics allows one to address mechanisms governed by the growth of mean-field instabilities, such as surface break-up processes, occurring at low energies [22,23,33], or volume (spinodal) decomposition, leading to multifragmentation events at Fermi energies [20,34].

The fluctuations implemented in the SMF model are essentially of thermal nature. Indeed, in semiclassical approaches quantal fluctuations cannot be accounted for. However, though the amplitude of fluctuations may be underestimated, the SMF model has been exploited to describe the development of surface instabilities (or metastabilities) characterizing heavy ion collisions around 10–20 MeV/nucleon, i.e., the formation of primary reaction products with large quadrupole and/or octupole deformation. As shown in Refs. [22,23], the analysis of shape observables, such as multipole moments, allows one to extract valuable information about fusion vs break-up probabilities, in low-energy semicentral reactions. Here we extend this kind of study to the possible occurrence of ternary break-up events, on which recent experimental investigations have been concentrated [10–12,35,36].

III. RESULTS

We focus on the study of the ^{197}Au + ^{197}Au reaction in the beam-energy range of 10–30 MeV/nucleon [10,12,35]. At 15 MeV/nucleon and at semicentral impact parameters, corresponding to strongly damped collisions [36], the data contain predominantly binary events. However, break-up processes into three or four massive fragments of comparable mass are also revealed. The ternary events are dominated by configurations where the heaviest fragment, close to the ^{197}Au mass, is recognized as the remnant of the projectile (PLF) or the target (TLF), while the other two fragments, indicated as F1 and F2 in the analysis of Ref. [35], are generated by the subsequent breakup of TLF or PLF.

The observed F1 and F2 fragments exhibit similar masses. Moreover, for the considered ternary partitioning mechanism, the three fragments are almost aligned along the axis determined by the TLF (or PLF) velocity and the velocity of the reconstructed PLF (or TLF). We notice that the latter feature is not compatible with the scenario of a pure statistical fission, pointing to a dynamical origin of the fragment formation mechanism. It is also observed that, in the majority of the events, the fragment with the largest parallel velocity (denoted as F1 in the experimental analysis) has the smallest mass.

The experimental study of the same system at higher beam energy (23 MeV/nucleon) identified a larger variety of fragment sizes [12]. Indeed, together with the observation of ternary events with fragments of comparable size, an abundant emission of intermediate mass fragments (IMF), with mass less than 30, accompanied by two heavy fragments (PLF and TLF), is observed in a large fraction of events. The decaying system keeps memory of the neck configuration and IMF's are emitted collinearly either from the neck side or from the opposite side along the separation axis (polar emission), as also seen in the reaction at 15 MeV/nucleon. Moreover, one observes that the intriguing process of the polar emission prevails for IMF's having mass larger than 50, whereas light IMF's exhibit features typical of the neck emission process, which becomes dominant and has been widely investigated at Fermi energies [13–17].

The aim of our theoretical analysis is to study the collision path leading to ternary break-up configurations, to probe the possible dynamical origin and the role of mean-field instabilities in the corresponding reaction mechanism. The nuclear reactions described above are investigated in the framework of the SMF model, using 100 test particles per nucleon, which ensure an accurate description of the mean-field dynamics. One hundred events are considered for each

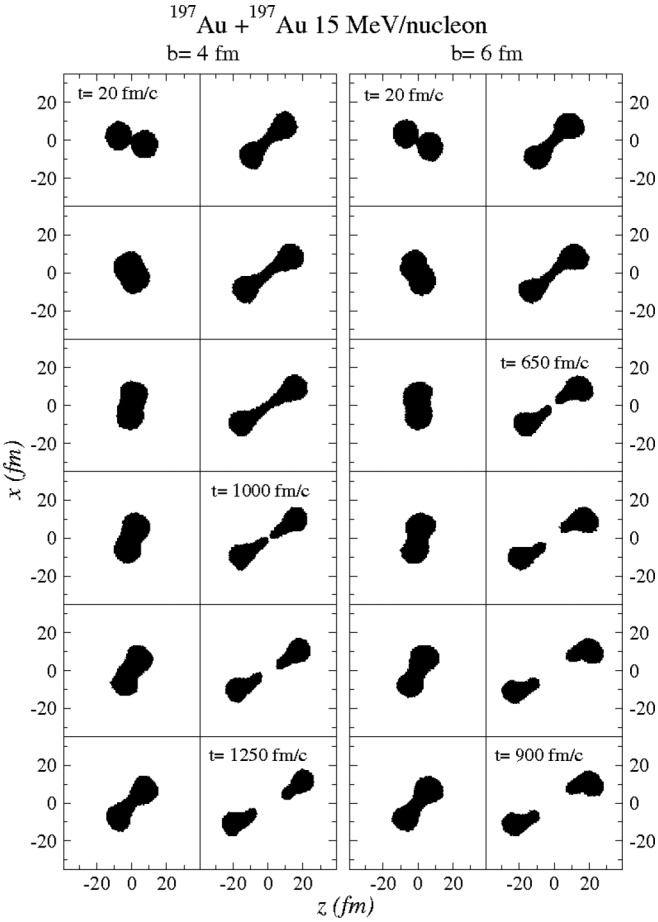

FIG. 1. Contour plots of the density projected on the reaction plane, calculated with SMF, for the reaction ^{197}Au + ^{197}Au at 15 MeV/nucleon, at several times, from top to bottom. The time instants corresponding to the splitting of the system in PLF-TLF fragments (t_{sep}) and to the final calculation time (t_{stop}) are indicated in the figure. Results corresponding to impact parameters $b = 4$ fm and $b = 6$ fm are displayed.

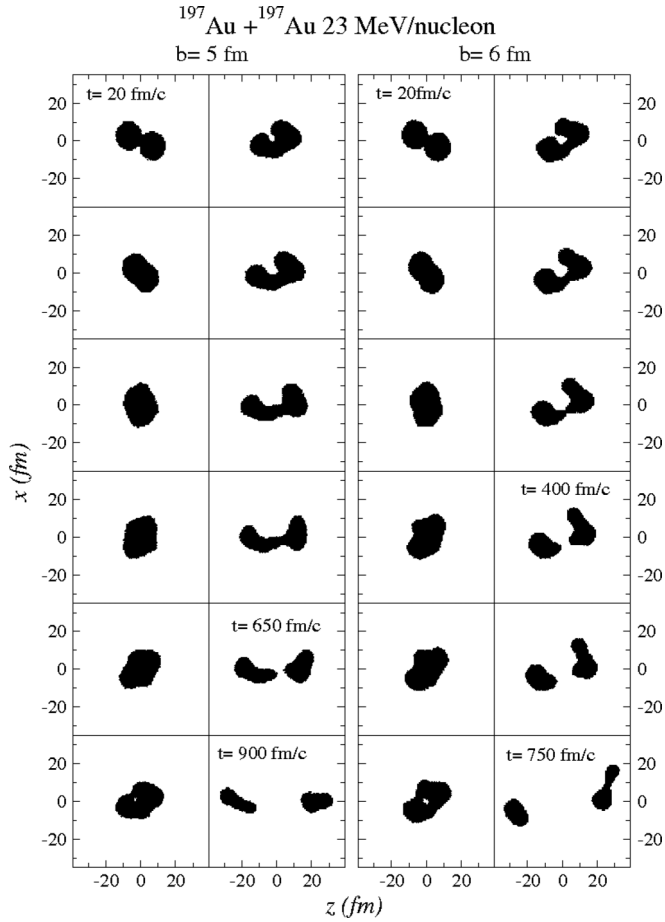

FIG. 2. The same as in Fig. 1 for the reaction at 23 MeV/nucleon. Results corresponding to impact parameters $b = 5$ fm and $b = 6$ fm are displayed.

set of macroscopic initial conditions (i.e., beam energy and impact parameter).

In Fig. 1 we present density contour plots (in the reaction plane) obtained in one event of the reaction ^{197}Au + ^{197}Au at 15 MeV/nucleon, for $b = 4$ fm (left panel) and $b = 6$ fm (right panel). The impact parameter region considered in our calculations, 4–6 fm, corresponds to rather dissipative collisions, where an intricate neck dynamics is perceived, leading eventually to the possibility of observing multiple breakup. Indeed, from the plots shown in Fig. 1, one can already appreciate that the reaction mechanism is heavily dominated by the occurrence of fragment quadrupole and octupole deformations in the exit channel. The neutron-rich neck region connecting the two reaction partners survives quite a long time (around $t = 500$–1000 fm/c), favoring the development of surface instabilities and mean-field fluctuations, leading to a variety of configurations for the reaction outcome. Rather deformed primary PLF-TLF are observed, which may split, by further breakup, into massive fragments of comparable size. This effect is quite pronounced in the impact parameter window considered, whereas for more central or more peripheral collisions, rather compact PLF-TLF fragments are emerging from the reaction path.

Figure 2 shows density contour plots obtained for the same reaction at 23 MeV/nucleon, $b = 5{,}6$ fm. Here fragmentation times become shorter and one can observe that the neck region is mostly absorbed by one of the two main fragments (PLF or TLF), inducing the formation of a rather elongated object, which may eventually break up, accompanied by a fragment of more compact shape.

A. Fragment recognition and PLF-TLF properties

As it can be noticed in Figs. 1 and 2, multiple breakup is not actually observed over the time scales (≈1000 fm/c) compatible with our dynamical description. This could be due to an overestimation of dissipative effects induced by nucleon emission [37] and/or to the approximate treatment of fluctuations in the SMF model [29]. The latter point could be cured by new methods to implement fluctuations in full phase space, which are presently under study [38]. A more effective fluctuating term is expected to lead to a faster dynamics, thus lowering energy dissipation and increasing the probability of observing a direct splitting of the system.

However, the time evolution of shape observables, such as quadrupole and octupole moments, of the primary fragments emerging from the reaction dynamics (see Figs. 1 and 2) can be used as an indicator of the occurrence of a subsequent breakup [22,23]. Indeed, a steadily increasing behavior of these shape observables, for a given fragment, can be associated with a large probability of finally observing its breakup in two pieces.

In the SMF model, the reaction products are reconstructed by applying a coalescence procedure to the one-body density $\rho(\mathbf{r})$, i.e., connecting neighboring cells, in coordinate space, with density $\rho(\mathbf{r}) > \rho_0/6$. In this way one can also identify a "gas" phase ($\rho(\mathbf{r}) < \rho_0/6$) associated with particles that leave rapidly the system (pre-equilibrium emission) and/or are evaporated [34]. Once fragments are identified, from the knowledge of the one-body distribution function, it is possible to calculate mass, charge, shape observables, and kinematical properties.

We first focus on the behavior of quadrupole $Q_2 = \int \rho(\mathbf{r_p})(3z_p^2 - r_p^2)d\mathbf{r_p}$ and octupole $Q_3 = \int \rho(\mathbf{r_p})z_p(5z_p^2 - 3r_p^2)d\mathbf{r_p}$ moments of PLF-TLF fragments. For each PLF-TLF fragment, we consider, in its center-of-mass frame, the three principal axes, (x_p, y_p, z_p), diagonalizing the coordinate tensor. In the new rotated frame, the z_p axis is chosen as the principal axis corresponding to the system maximum elongation. The orientation of the z_p axis is chosen in such a way that $\cos(\theta_p)$ is positive (negative) for PLF (TLF) fragments, being θ_p the angle between the z_p axis and the beam direction (z) axis. However, in the following the absolute value of the octupole moment, $|Q_3|$, will be considered.

We will denote, in each event, as DF (deformed fragment) the one exhibiting the largest deformation, which may eventually break up, and as SF (spherical fragment) the other one. Note that in some events both fragments can be deformed. Actually, the latter situation is more likely at the lower energy (15 MeV/nucleon), whereas at 23 MeV/nucleon the two fragments exhibit a different shape; see Figs. 1 and 2.

Figure 3 represents the average Q_2 and $|Q_3|$ values of the primary fragments issued from the reaction at 23 MeV/nucleon, $b = 6$ fm, as a function of time. Error bars reported in the figure are associated with the variance evaluated over the 100 events considered. In the figure, the initial time ($t_{\rm sep}$) corresponds to the instant when the composite system splits into PLF and TLF fragments. As already suggested by the plots shown in Fig. 2, one observes that whereas the shape of one of the two primary fragments (the SF fragment) keeps stabilized around rather low Q_2 and $|Q_3|$ values, the deformation of the other fragment (DF), which has absorbed the neck region, increases with time, reaching a kind of saturation around $t - t_{\rm sep} \approx 300$ fm/c.

We follow the reaction dynamics until $t_{\rm stop} = 1250(900)$ fm/c for the collisions at 15 MeV/nucleon, $b = 4(6)$ fm and $t_{\rm stop} = 900(750)$fm/c at 23 MeV/nucleon, $b = 5(6)$ fm. At this considered final time, PLF and TLF are well separated and the development of shape deformation is clearly evidenced. Thus we assume that after the DF has reached its maximum degree of deformation it will likely split in two pieces, though we cannot provide a precise estimation

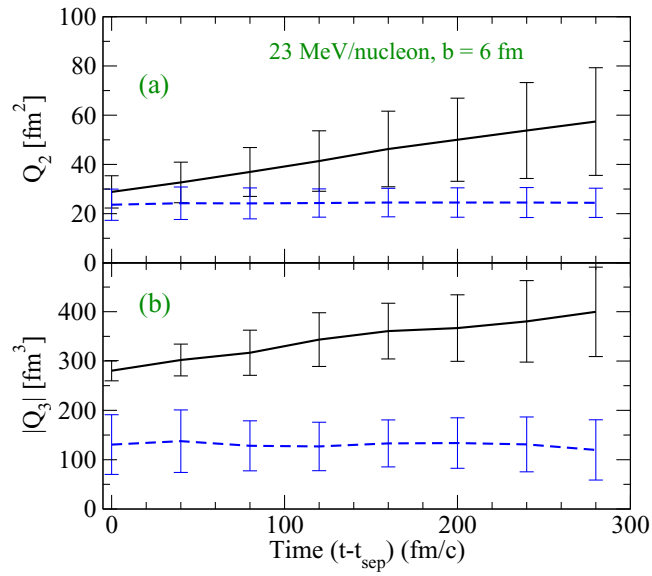

FIG. 3. (Color online) Time evolution of the average quadrupole (a) and octupole (b) moments of DF (full line) and SF (dashed line) fragments (see text) obtained in the ^{197}Au + ^{197}Au reaction at 23 MeV/nucleon, $b = 6$ fm.

of the breakup instant and of the corresponding degree of alignment of the three fragments.

Figure 4(a) shows the PLF-TLF distribution, evaluated at $t_{\rm stop}$, in the plane determined by parallel and transverse velocities, for the reaction at 23 MeV/nucleon, $b = 5$–6 fm.

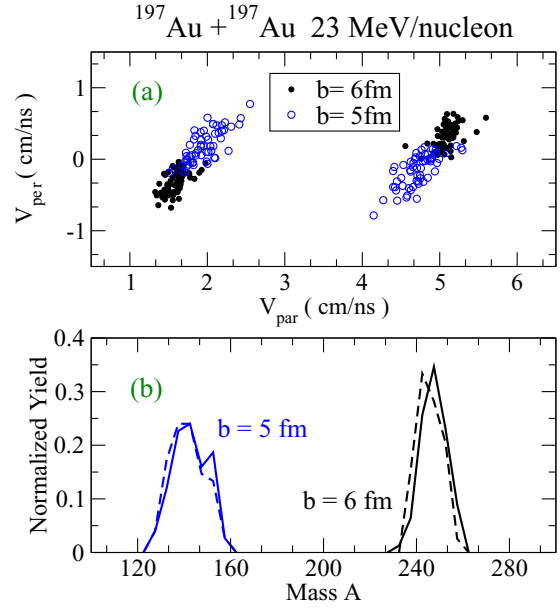

FIG. 4. (Color online) (a) Distribution in the plane determined by parallel and transverse velocities of PLF and TLF fragments issued from the ^{197}Au + ^{197}Au reaction, at 23 MeV/nucleon, $b = 5$–6 fm. (b) Mass distribution, normalized to the number of events, of DF (full line) and SF (dashed line) fragments for the same reactions indicated above. For the reaction at $b = 6$ fm, the fragment masses are shifted by 100 units in the figure, for better visibility.

A stronger dissipation, with respect to the data [11], is observed. However, we stress that our analysis is focused on dynamical ternary breakup mechanisms, occurring at semicentral collisions ($b = 5$–6 fm), in a window where the results exhibit a large dependence on the impact parameter (see Fig. 4). On the other hand, the experimental ternary break-up data [11] also contain the contribution of the PLF-TLF statistical decay, which may also take place at more peripheral impact parameters. Thus, apart from the problems related to the overestimated dissipation in SMF, a direct comparison to data is not straightforward and is beyond the aim of the present manuscript.

Figure 4(b) displays the mass distribution of DF and SF fragments. It is possible to observe that the mass of the DF fragment is shifted to larger values, though the effect is not so pronounced. Moreover, we find for the PLF-TLF fragments an average mass of ≈150 units, indicating the occurrence of a more abundant nucleon emission (due to pre-equilibrium effects and/or evaporation) with respect to the experimental data, reporting larger masses for PLF-TLF [10,39]. It should be noticed that, at the separation time t_{sep}, PLF-TLF fragments are still excited and have intrinsic angular momentum. For the DF fragment, we find excitation energies, E^*, of the order of 100 MeV (±50 MeV) for the reactions at 15 MeV/nucleon and 400 MeV (±100 MeV) for the reactions at 23 MeV/nucleon. The intrinsic spin J is in the ranges of 20–40 $\hbar$ at 15 MeV/nucleon and 80–130 $\hbar$ at 23 MeV/nucleon.

We then concentrate our analysis on the DF fragments and estimate their most probable break-up configuration, as explained below and represented in Fig. 5.

The prescription, based on the recognition of density bumps and employed to identify fragments in collisions at higher energies [34], is extended here to systems which are neck shaped, looking at the density profile along the axis of maximum deformation. For each event, we first evaluate the center of mass of the largest agglomerate inside the DF fragment, corresponding to the maximum reached by the density profile along its principal, z_p, axis direction. Then we calculate the corresponding nucleon number, $A2_{\rm half}$, integrating the density from the left extreme up to the center (for a fragment orientation as shown in Fig. 5). The masses of the largest (A2) and smallest (A1) fragments which may originate from the breakup of the DF fragments are evaluated as $A2 = 2A2_{\rm half}$ and $A1 = A_{\rm DF} - A2$, where $A_{\rm DF}$ is the total mass of the primary DF fragment. The same procedure is followed to evaluate the charge of the two fragments.

B. Fragment properties in ternary breakup

Let us consider first the reaction at 15 MeV/nucleon. In this case the neck rupture is almost symmetric between PLF and TLF, leading to the formation of two deformed fragments in the majority of the events. Since we are interested in ternary events, possible break-up configurations are considered only for one of the two fragments at a time. Moreover, generally speaking, the probability that both fragments eventually break up, leading to quaternary events, should be much smaller than the probability of observing just one rupture.

Figure 6(a) shows the mass distribution of the lightest, A1, and heaviest, A2, fragments identified with the method outlined above, for the impact parameter $b = 5$ fm. Very similar results are obtained for other impact parameters inside the considered window (4–6 fm). Once the masses are normalized to the average mass of the DF fragments, results look close to the experimental distributions (see Refs. [35,39]).

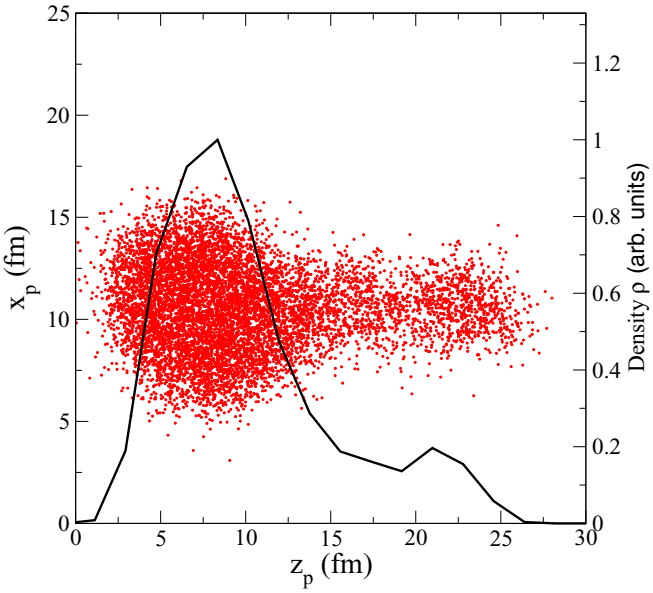

FIG. 5. (Color online) Illustration of the fragment recognition procedure adopted in the calculations: Density distribution of a DF fragment in the plane determined by its principal axis z_p and the corresponding transverse axis. The full line denotes the density profile along the z_p axis (in arbitrary units).

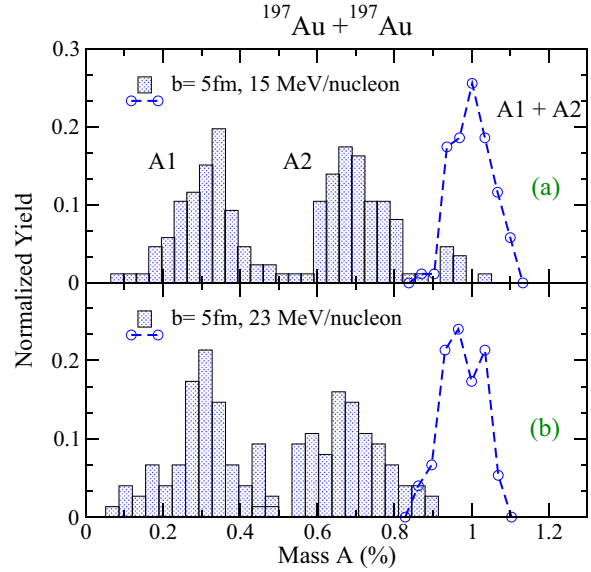

FIG. 6. (Color online) Mass distribution of the fragments A1 and A2 and of their sum (DF fragment), emerging from the breakup of the DF fragment, for the reaction ^{197}Au + ^{197}Au at (a) 15 and (b) 23 MeV/nucleon. A1 denotes the smallest fragment. Masses are normalized to the average mass of the DF fragment.

In particular, the calculations are able to reproduce the distance between the peaks of the A1 and A2 mass distributions, which amounts to about 30% of the DF mass. The width of the mass distributions is also compatible with the experimental results. This agreement can be considered as nice evidence that the ternary partitioning in comparable masses comes from the reaction dynamics associated with semicentral impact parameters. However, a lack of events corresponding to symmetric ruptures is observed in the simulations. This comes from the fact that statistical fission processes of PLF-TLF fragments are neglected in our analysis, which only focus on break-up mechanisms of dynamical origin. On the other hand, this contribution is contained in the data.

Similar results have been recently reported in the context of the improved quantum molecular dynamics (ImQMD) calculations of Ref. [40], where a detailed comparison with the experimental findings of Ref. [39] is presented.

Results obtained at the higher bombarding energy of 23 MeV/nucleon are shown in the panel (b) of the Fig. 6 As already discussed above, in addition to the partitions observed at 15 MeV/nucleon, a relevant IMF emission is also seen in the experimental data [11]. In the calculations, we observe (see Fig. 2) the occurrence of larger surface instabilities characterizing the neck region, from which small fragments could also originate. However, ternary break-up events, with fragments of comparable masses, are also quite likely, corresponding to configurations where the DF fragment is systematically enriched in mass (see Fig. 4). The behavior observed for the mass distribution of fragments A1 and A2 is quite close to the one obtained at 15 MeV/nucleon. However, larger variances, reflecting the more dissipative dynamics, are observed.

It should be noticed that in the calculations of Ref. [40], as well as in our SMF simulations at 15 MeV/nucleon, the lightest fragment (A1) emerges mainly from the neck region (see also Fig. 1), thus being located at midvelocity. On the other hand, in the data analysis reported in Ref. [35], the fragment with the largest parallel velocity (F1) has the smallest mass. Also in the data at 23 MeV/nucleon [12], this polar emission mechanism dominates for massive fragments.

In the SMF simulations, this feature seems to be present at 23 MeV/nucleon. In fact, as one can notice in Fig. 2, owing to increased angular momentum effects, the DF fragment rotates before it reaches its maximum deformation and a subsequent breakup may take place. As a consequence, in the case of a PLF breakup for instance, the lightest fragment may emerge with large positive parallel velocity. Indeed, at the moment of its breakup, the deformed PLF may be oriented, in coordinate space, in such a way that the matter absorbed from the neck appears located on the right side with respect to the axis connecting TLF and PLF (as in the configuration of Fig. 5, for instance). Then, to establish a closer connection with the experimental analysis of Ref. [35], in our fragment recognition procedure we now identify as F1 the fragment which is located on the external side of the DF fragment [i.e., on its right (left) side in the case of the PLF (TLF) breakup], and as F2 the other one. The corresponding mass distribution is shown in Fig. 7.

The simulations show an interesting evolution, with the impact parameter, towards the features observed experimentally. Indeed, whereas at $b = 5$ fm the F1 fragment exhibits

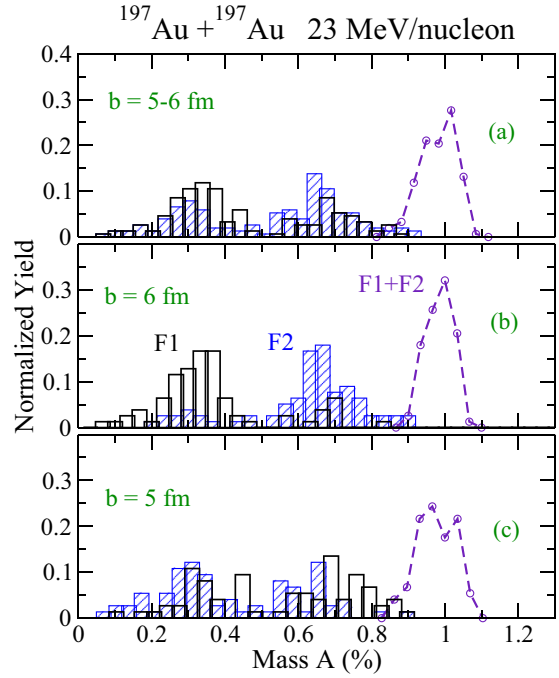

FIG. 7. (Color online) Mass distributions of fragments F1 (black histogram) and F2 (blue [gray] histogram), and of their sum (dashed line), as obtained in the reaction ^{197}Au + ^{197}Au at $b = 5$ fm (c) and $b = 6$ fm (b). Panel (a) represents the distribution corresponding to the geometrical weight of the two impact parameters. Masses are normalized to the average mass of the DF fragment.

a wide mass distribution, at $b = 6$ fm it is mostly located in the low-mass region. These results point to the occurrence of a reaction mechanism, i.e., neck rupture coupled to angular momentum effects, which could explain the experimental observation. Figure 7(a) of the figure represents the distribution corresponding to the geometrical weight of the two impact parameters.

As mentioned above, a significant influence of angular momentum effects on the reaction mechanism starts to be noticed at 23 MeV/nucleon, whereas in the data this effect is already present at 15 MeV/nucleon [35]. It is also interesting to observe that, according to the simplified BL approach adopted in Ref. [22], where thermal fluctuations are implemented in the evolution of shape observables, excitation energy and angular momentum of the deformed PLF-TLF fragments as obtained in the reaction at 15 MeV/nucleon at t_{sep} would be too low to produce a fast breakup. On the other hand, the PLF-TLF properties predicted by SMF simulations at 23 MeV/nucleon would be compatible with rupture times $(t - t_{sep})$ of the order of 300 fm/c and the occurrence of a preferential emission direction (see Fig. 5 of Ref. [22]). We notice that similar final times, estimated on the basis of the saturation of Q_2 and $|Q_3|$ values (see Fig. 3), are considered in our fragment recognition procedure.

This shift of beam energy may be due to the overestimated dissipation by nucleon emission, which is a drawback of SMF calculations at the considered beam energies [37]. Indeed, the latter may quench thermal and angular momentum

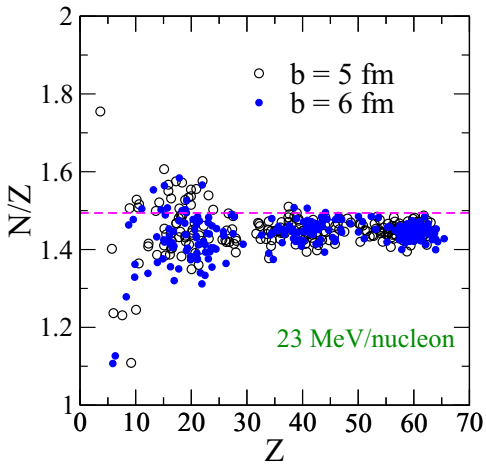

FIG. 8. (Color online) N/Z ratio, as a function of the fragment charge, as obtained for the reactions at 23 MeV/nucleon, $b = 5$–6 fm. The scattered points correspond to the simulated events. The dashed line represents the system initial asymmetry $N/Z = 1.49$.

effects. Moreover, as stressed above, the effect of dynamical fluctuations, which could speed up the system breakup, is underestimated in the SMF approach, where fluctuations are projected in coordinate space [29]. A shift, with respect to data, of the beam energy threshold associated with dynamical fragmentation has been observed also for SMF simulations of central collisions at higher energies [41]. On the other hand, in QMD-like calculations rotational effects could be missing because of the too fast reaction dynamics and the reduced mean-field effects [34,40].

Finally, we move to discuss the isotopic features of the ternary break-up events. Figure 8 displays the relation between the N/Z ratio and the charge number Z of the three fragments obtained, in the case of the reaction at 23 MeV/nucleon, $b = 5{,}6$ fm. As a general trend, we observe that the average N/Z ratio of the whole system at the final time, which amounts to $N/Z \approx 1.43$, is lower than the system initial asymmetry ($N/Z = 1.49$ for Au nuclei), reflecting pre-equilibrium neutron-rich emission and/or evaporation. One can also see that, especially in the case of the more peripheral impact parameter ($b = 6$ fm), the lightest fragments are slightly more proton rich. This may be due to Coulomb polarization effects, because, as explained before, light fragments are located in this case at the outer side of the system. However, more statistics would be needed in order to reach firm conclusions about this point.

IV. CONCLUSIONS

We have undertaken an analysis of new fragmentation modes, on which recent experimental investigations have been concentrated, which may develop in low-energy heavy ion collisions. The possibility of observing ternary breakup processes of dynamical origin is explored within the SMF model, looking at the concurrent role of surface mean-field instabilities, dissipative and angular momentum effects. Indeed, large quadrupole and octupole deformation effects are developing in binary exit channels of semicentral reactions, which may lead to a subsequent breakup of the PLF-TLF fragments. The procedure based on the study of shape deformations, which was introduced in Ref. [23] to evaluate fusion vs breakup cross sections, is extended here to the search of multiple breakup processes. Moreover, a fragment recognition method is introduced to identify the most probable break-up configurations associated with deformed PLF-TLF fragments. For reactions at ≈20 MeV/nucleon, SMF calculations are able to explain the main features observed experimentally for ternary break-up events, namely mass partitions and the appearance of preferential emission directions. The model also indicates that these features emerge from a delicate balance between the neck dynamics and rotational effects. Thus the analysis of these fragmentation modes allows one to get a deeper insight into the nature of dissipation mechanisms and the properties of the nuclear effective interaction. However, a self-consistent improved dynamical description would be desirable, aiming at explaining the features observed also at lower energies [35]. Efforts in the direction of implementing fluctuations, in full phase space, in dynamical mean-field models are currently being developed [38]. Moreover, it would be extremely interesting to extend this kind of investigations to reactions involving neutron-rich (or even exotic) nuclei [18]. Indeed, the reaction dynamics could be affected by the neutron enrichment of the neck region, related to neutron skin effects and/or isospin migration mechanisms [15,21]. One would also expect a sensitivity of the reaction mechanism, and of the features of the emitted fragments, to the isovector terms of the nuclear potential, opening interesting perspectives towards the extraction of new, independent information on the density behavior of the nuclear symmetry energy [19].

ACKNOWLEDGMENT

This work, for V. Baran, was supported by a grant of the Romanian National Authority for Scientific Research, CNCS-UEFISCDI, Project No. PN-II-ID-PCE-2011-3-0972.

[1] P. Lautesse *et al.*, Eur. Phys. J. A **27**, 349 (2006).
[2] T. C. Awes *et al.*, Phys. Rev. Lett. **52**, 251 (1984).
[3] V. Penumetcha *et al.*, Phys. Rev. C **42**, 1489 (1990).
[4] K. Washiyama, S. Ayik, and D. Lacroix, Phys. Rev. C **80**, 031602 (2009).
[5] G. Casini *et al.*, Phys. Rev. Lett. **83**, 2537 (1999); F. Amorini *et al.*, *ibid.* **102**, 112701 (2009).
[6] M. Colonna, M. Di Toro, and A. Guarnera, Nucl. Phys. A **589**, 160 (1995).
[7] C. Simenel, Eur. Phys. J. A **48**, 152 (2012).
[8] P. Glassel, D. V. Harrach, H. J. Specht, and L. Grodzins, Z. Phys. A **310**, 189 (1983).
[9] A. A. Stefanini *et al.*, Z. Phys. A **351**, 167 (1995).
[10] I. Skwira-Chalot *et al.*, Phys. Rev. Lett. **101**, 262701 (2008).

[11] T. Cap, K Siwek-Wilczyńska, I. Skwira-Chalot, and J. Wilczyński (CHIMERA Collaboration), Phys. Scr. **T154**, 014007 (2013).
[12] T. Cap *et al.*, Phys. Scr. **89**, 054005 (2014).
[13] V. Baran, M. Colonna, M. Di Toro, Nucl. Phys. A **730**, 329 (2004).
[14] E. De Filippo *et al.*, Phys. Rev. C **71**, 044602 (2005).
[15] E. De Filippo *et al.* (Chimera Collaboration), Phys. Rev. C **86**, 014610 (2012).
[16] K. Brown *et al.*, Phys. Rev. C **87**, 061601 (2013).
[17] S. Barlini *et al.* (FAZIA Collaboration), Phys. Rev. C **87**, 054607 (2013).
[18] P. Cammarata *et al.*, Nucl. Instrum. Methods Phys. Res., Sect. A **761**, 1 (2014).
[19] B.-An Li, A. Ramos, G. Verde, and I. Vidaña, Eur. Phys. J. A **50**, 9 (2014).
[20] Ph. Chomaz, M. Colonna, and J. Randrup, Phys. Rep. **389**, 263 (2004).
[21] V. Baran, M. Colonna, V. Greco, and M. Di Toro, Phys. Rep. **410**, 335 (2005).
[22] L. Shvedov, M. Colonna, and M. Di Toro, Phys. Rev. C **81**, 054605 (2010).
[23] C. Rizzo, V. Baran, M. Colonna, A. Corsi, and M. Di Toro, Phys. Rev. C **83**, 014604 (2011).
[24] S. Ayik and C. Gregoire, Phys. Lett. B **212**, 269 (1988).
[25] J. Rizzo, P. Chomaz, and M. Colonna, Nucl. Phys. A **806**, 40 (2008), and references therein.
[26] V. Baran *et al.*, Nucl. Phys. A **703**, 603 (2002).
[27] B. Borderie and M. F. Rivet, Prog. Part. Nucl. Phys. **61**, 551 (2008), and references therein.
[28] A. Guarnera, M. Colonna, and Ph. Chomaz, Phys. Lett. B **373**, 267 (1996).
[29] M. Colonna *et al.*, Nucl. Phys. A **642**, 449 (1998).
[30] V. Baran *et al.*, Nucl. Phys. A **600**, 111 (1996).
[31] M. Papa *et al.*, Phys. Rev. C **68**, 034606 (2003); **72**, 064608 (2005).
[32] J. Tian *et al.*, Chin. Phys. C **33**, 109 (2009) ; J. Tian, X. Wu, Z. Li, K. Zhao, Y. Zhang, X. Li, and S. Yan, Phys. Rev. C **82**, 054608 (2010).
[33] D. Boilley, E. Suraud, Y. Abe, and S. Ayik, Nucl. Phys. A **556**, 67 (1993).
[34] M. Colonna, A. Ono, and J. Rizzo, Phys. Rev. C **82**, 054613 (2010); J. Rizzo, M. Colonna, and A. Ono, *ibid.* **76**, 024611 (2007).
[35] J. Wilczynski *et al.*, Phys. Rev. C **81**, 024605 (2010).
[36] J. Wilczynski *et al.*, Phys. Rev. C **81**, 067604 (2010).
[37] D. Lacroix and Ph. Chomaz, Nucl. Phys. A **636**, 85 (1998).
[38] P. Napolitani and M. Colonna, Phys. Lett. B **726**, 382 (2013).
[39] I. Skwira-Chalot *et al.*, Int. J. Mod. Phys. E **15**, 495 (2006); **16**, 511 (2007).
[40] Y. Li, S. Yan, X. Jiang, and L. Wang, Nucl. Phys. A **902**, 1 (2013).
[41] E. Bonnet, M. Colonna, A. Chbihi, J. D. Frankland, D. Gruyer, and J. P. Wieleczko, Phys. Rev. C **89**, 034608 (2014).